BRAIN COMMUNICATIONS

Cholinergic and inflammatory phenotypes in transgenic tau mouse models of Alzheimer's disease and frontotemporal lobar degeneration

Anna L. Cranston,[1,*] Adrianna Wysocka,[2,*] Marta Steczkowska,[3] Maciej Zadrożny,[3] Ewelina Palasz,[3] Charles R. Harrington,[1,4] Franz Theuring,[5] Claude M. Wischik,[1,6] Gernot Riedel[1,†] and Grazyna Niewiadomska[2,†]

---

*,†These authors contributed equally to this work.

An early and sizeable loss of basal forebrain cholinergic neurons is a well-characterized feature associated with measurable deficits in spatial learning and cognitive impairment in patients with Alzheimer's disease. In addition, pro-inflammatory glial cells such as astrocytes and microglia may play a key role in the neurodegenerative cascade of Alzheimer's disease and tauopathies. We recently presented two mouse models: Line 1, expressing the truncated tau fragment identified as the core of the Alzheimer's paired helical filament, and Line 66, expressing full-length human tau carrying a double mutation (P301S and G335D). Line 1 mice have a pathology that is akin to Alzheimer's, whilst Line 66 resembles frontotemporal lobar degeneration. However, their cholinergic and inflammatory phenotypes remain elusive. We performed histological evaluation of choline acetyltransferase, acetylcholinesterase, p75 neurotrophin receptor, microglial ionized calcium binding adaptor molecule 1 and astrocytic glial fibrillary acidic protein in the basal forebrain, hippocampus and cortex of these models. A significant lowering of choline acetyltransferase-positive neurons and p75-positive neurons in the basal forebrain of Line 1 at 3, 6 and 9 months was observed in two independent studies, alongside a significant decrease in acetylcholinesterase staining in the cortex and hippocampus. The reductions in choline acetyltransferase positivity varied between 30% and 50% at an age when Line 1 mice show spatial learning impairments. Furthermore, an increase in microglial ionized calcium binding adaptor molecule 1 staining was observed in the basal forebrain, hippocampus and entorhinal cortex of Line 1 at 6 months. Line 66 mice displayed an intact cholinergic basal forebrain, and no difference in p75-positive neurons at 3 or 9 months. In addition, Line 66 exhibited significant microglial ionized calcium binding adaptor molecule 1 increase in the basal forebrain and hippocampus, suggesting a prominent neuroinflammatory profile. Increased concentrations of microglial interleukin-1β and astrocytic complement 3 were also seen in the hippocampus of both Line 1 and Line 66. The cholinergic deficit in Line 1 mice confirms the Alzheimer's disease-like phenotype in Line 1 mice, whilst Line 66 revealed no measurable change in total cholinergic expression, a phenotypic trait of frontotemporal lobar degeneration. These two transgenic lines are therefore suitable for discriminating mechanistic underpinnings between the Alzheimer's and frontotemporal lobar degeneration-like phenotypes of these mice.

1 School of Medicine, Medical Sciences and Nutrition, University of Aberdeen, Foresterhill, Aberdeen AB25 2ZD, UK
2 Nencki Institute of Experimental Biology, Polish Academy of Science, Warsaw 02-093, Poland
3 Mossakowski Medical Research Centre, Warsaw 02-106, Poland
4 TauRx Therapeutics Ltd, Foresterhill, Aberdeen AB25 2ZP, UK
5 Institute of Pharmacology, Charite—Universitätsmedizin Berlin, Berlin, Germany
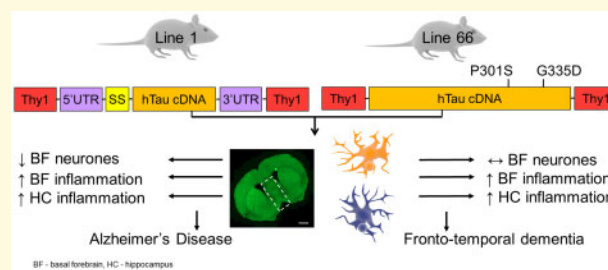6 TauRx Therapeutics Ltd, Aberdeen AB24 5RP, UK

Correspondence to: Gernot Riedel, PhD Institute of Medical Sciences, University of Aberdeen,
Foresterhill, Aberdeen AB25 2ZD, UK
E-mail: g.riedel@abdn.ac.uk

Correspondence may also be addressed to: Grazyna Niewiadomska, PhD Laboratory of Preclinical
Studies in Neurodegenerative Diseases, Nencki Institute of Experimental Biology, 3 Pasteur Street,
02-093 Warsaw, Poland
E-mail: g.niewiadomska@nencki.gov.pl

Graphical Abstract

Introduction

Tauopathies are a diverse group of neurodegenerative dis-
orders associated with cognitive and behavioural impair-
ments in the ageing population. The most prevalent,
Alzheimer's disease, is a complex and heterogeneous neu-
rodegenerative disease of the CNS, first presented by
German psychiatrist Alois Alzheimer (Alzheimer, 1907),
typically characterized by the deposition of extracellular
β-amyloid plaques and intracellular tau neurofibrillary tan-
gles (NFTs). Tau is a low-molecular-weight microtubule-
associated protein, expressed predominantly in axons
(Buee et al., 2000) and also dendrites (Ittner and Ittner,
2018). Tau regulates the assembly and stability of microtu-
bules, and its microtubule-binding function is regulated
negatively through phosphorylation (Weingarten et al.,
1975). In Alzheimer's disease, tau accumulates as NFTs
and ultimately into paired helical filaments. The core of
the paired helical filament is composed of a truncated 95-
amino-acid fragment of tau (Wischik et al., 1988) and is
capable of catalytic conversion of normal soluble tau into
intracellular oligomeric aggregates (Wischik et al., 1995,
1996), resulting in dystrophic neurites, dendrites and cell
bodies, a characteristic pathology of tauopathies (Spires-
Jones et al., 2009). The role of phosphorylation in this
process remains unknown (Kimura et al., 2018).

A significant loss of up to 50% of basal forebrain cho-
linergic neurons is another well-characterized feature of
Alzheimer's disease (Davies and Maloney, 1976; Perry
et al., 1985). Acetylcholine plays a crucial role in the per-
ipheral nervous system and central nervous system and
can be measured by the presence of neuronal choline ace-
tyltransferase (ChAT; Nagai et al., 1983). In addition, an
age-dependent decline in acetylcholinesterase (AChE), the
enzyme responsible for acetylcholine hydrolysis (Ferreira-
Vieira et al., 2016), is associated with reduced AChE in
patients with Alzheimer's disease (Hirano et al., 2012;
Janeczek et al., 2018). As such, current symptomatic
Alzheimer's disease treatments, specifically AChE inhibi-
tors donepezil and rivastigmine, act to remediate this cho-
linergic dysfunction through increasing the level of
acetylcholine at the synaptic cleft (Raina et al., 2008).

Intriguingly, cholinergic degeneration is lacking in fron-
totemporal lobar degeneration (FTLD), a progressive neu-
rodegenerative tauopathy primarily affecting the frontal
and temporal lobes of the brain (Wilkinson et al., 2002;
Roy et al., 2016). This has further strengthened the argu-
ment favourably towards the 'Cholinergic Hypothesis' of
Alzheimer's disease (Terry and Buccafusco, 2003) and is
supported by histological post-mortem studies showing
that low-affinity p75 neurotrophin receptor (p75^{NTR}), a
marker of cholinergic basal forebrain neurons, is signifi-
cantly reduced in mild cognitive impairment (Mufson
et al., 2002). Therefore, an in-depth understanding of the
cholinergic system is key to deciphering the pathological
dissociation between Alzheimer's disease and other

tauopathies. The basal forebrain cholinergic system is composed of the medial septum (MS), horizontal limb of the diagonal band of Broca (HDB) and vertical limb of the diagonal band of Broca (VDB), nucleus basalis of Meynert (classified as the nucleus basalis magnocellularis in the murine brain; nBM), nucleus accumbens and the substantia innominata (Niewiadomska et al., 2009). As a network, these regions provide the major cholinergic projections via the septo-hippocampal pathway to the entorhinal cortex (EC) and hippocampus, regions that exhibit parallel tau pathology (Niewiadomska et al., 2006). Afferent cholinergic projections from the MS to hippocampus have been shown as a critical pathway in mediating spatial and mnemonic function (Robinson et al., 2010; Deiana et al; 2011; Okada et al., 2015).

Several tau transgenic (Tg) mouse models have been generated (Götz et al., 2001; Yanamandra et al., 2015) to explain the pathogenic mechanisms of tau and to assess the efficacy of therapeutic targets for Alzheimer's disease and FTLD. Familial autosomal dominantly inherited MAPT mutations provide a basis for the majority of tau Tg mouse models generated to date. These include a tau Tg mouse that overexpresses tau carrying the mutation P301L (Götz et al., 2001), a mutation associated with FTLD (Caillet-Boudin et al., 2015). Overexpression of human P301L tau in cortical and hippocampal neurons increases astrocytosis in addition to neuronal apoptosis, similar to those observed in human tauopathies (Götz et al., 2001). Alternative approaches to the P301L model have explored the overexpression of human wild-type (WT) tau in mice, observing synapse loss and microglial activation, in some cases even preceding the deposition of intracellular NFTs (Yoshiyama et al., 2007). A limitation of the P301L model is that these animals exhibit motor deficits and hind limb paralysis, traits that are not consistent with symptoms observed in patients with Alzheimer's disease. Also, microglial activation without the appearance of NFT pathology can frequently be observed in these mice (Götz et al., 2001), presenting a model lacking true translational features.

The cholinergic Alzheimer's disease-like dysfunction has been characterized for several Tg rodent tau models, most recently in the THY-Tau22 mouse, a model that displayed major hippocampal Alzheimer's disease-like tau pathology within the septo-hippocampal pathway (Belarbi et al., 2009). This model also presented a significant reduction in ChAT-immunoreactive neurons in the MS. Furthermore, an age-dependant mild astrogliosis was reported in THY-Tau22 mice, particularly in association with tau-positive cells (Schindowski et al., 2006).

A pro-inflammatory activation of microglia and astrocytes has recently been identified to play a key role in acting as secondary effector in neurodegenerative cascades in the human brain, with neuroinflammation considered to precede the onset of both Alzheimer's disease and FTLD symptoms in patients (Heneka et al., 2014; Morales et al., 2014). This is consistent with observations

in P301L tau Tg mice (Götz et al., 2001). In patients with Alzheimer's disease, a strong correlation exists between NFT deposition and density of activated microglia, typically established through immunohistochemical staining of the ionized calcium binding adaptor molecule 1 (Iba1), a robust marker of neuroinflammation (Arends et al., 2000). In addition, increased inflammatory mediators, such as tumour necrosis factor alpha and interleukin-1 beta (IL-1β), are correlated with cognitive deficits for patients with late-stage Alzheimer's disease (Morimoto et al., 2011). In particular, sustained IL-1β overexpression secreted by activated microglia is known to exacerbate tau pathology in tau-overexpressing mice (Ghosh et al., 2013) and up-regulation of complement C3 protein, a marker of activated A1 astrocytes, has been observed in PS19 mice in response to NFT pathology (Litvinchuk et al., 2017).

Current animal models of tauopathy and Alzheimer's disease fail to address the specific molecular mechanisms by which products of inflammation produced through activated microglia and astrocytes can induce Alzheimer's disease neurodegeneration and the potential link between the observed cholinergic basal forebrain degeneration. Therefore, we conducted a robust evaluation of the cholinergic system of Line 1 (L1) and Line 66 (L66) Tg mice to decipher the phenotypic differences in these two genetically distinct models. Given the pathological and behavioural phenotypes previously described in these models (Melis et al., 2015), the cholinergic phenotypes were performed in two independent studies undertaken in Warsaw, Poland, and Aberdeen, UK, alongside a robust evaluation of the neuroinflammatory phenotype of these two Tg mouse models.

Materials and Methods

Tg animals

Female homozygous Tg L1, L66 and WT NMRI litters were generated as previously described (Melis et al., 2015). All animals were bred commercially at Charles River, UK, and distributed to the respective facilities (road for Aberdeen, air-freight for Warsaw) 1 month prior to use to allow ample acclimatization. Animals were colony housed (up to four per cage) in wire-lid cages (Makrolon II) on corn cob bedding and enrichment (paper strips and cardboard tubes) in a controlled facility (temperature 20–22°C, 60–65% humidity, air changes: 17–20 changes per hour) and ad libitum access to water and food pellets and under a 12-h light/dark cycle (lights on at 07:00 am). Experiments were carried out in accordance with the European Communities Council Directive (63/2010/EU), a project licence with local ethical approval under the UK Animals (Scientific Procedures) Act (1986), or with approval from First Warsaw Local Ethics Committee for Animal Experimentation, and carried out

in accordance with Polish Law on the Protection of Animals and National Institute of Health's Guide for Care and Use of Laboratory Animals (Publication No. 85-23, revised 1985).

Immunohistochemistry

Brains were processed independently from mice aged 3, 9 and 12 months (± 2 weeks) in Warsaw, Poland, and at 6 months (± 2 weeks) in Aberdeen, UK. Immunohistochemical analyses were carried out in independent studies in Aberdeen, UK [ChAT, Iba1, glial fibrillary acidic protein (GFAP)], and Warsaw, Poland (ChAT, p75^{NTR}, AChE).

Fluorescent immunohistochemistry for ChAT, Iba1 and GFAP (Aberdeen)

Adult female homozygous 6-month-old Tg L1, L66 and WT NMRI mice were randomly selected for terminal intraperitoneal injection of pentobarbital (Euthatal; 0.2 ml/30 g body weight; Merial Animal Health Ltd, Lyon, France). Anaesthetized mice were transcardially perfused with 0.9% (w/v) saline, followed by 4% paraformaldehyde (Sigma-Aldrich, UK) until fixation was achieved. Skulls were immediately dissected, and whole brains removed and post-fixed in 4% paraformaldehyde (4 h), followed by 24 h incubation in 10% sucrose (Phosphate buffered saline (PBS); pH = 7.4), 30% sucrose (PBS) and 2% DMSO/2% glycerol (Sigma-Aldrich) at 4°C over 3 days. Following post-fixation, brains were snap-frozen in isopentane (2-methylbutane; Sigma-Aldrich).

Free-floating sections were used from whole brains embedded in OCT matrix (CellPath Ltd, Newtown, UK). Coronal sections (30 µm) were obtained (CM1850 Cryostat; Leica Biosystems) from brain regions of interest ['Bregma 1.4'; 'Bregma −3.64 mm', according to Paxinos and Franklin (2001)] and stored in cryoprotectant solution (glycerol, ethylene glycol, 0.1 M PB, 1:1:2) until staining. Every second section (nBM, VDB) or every third section [MS, HDB, striatum (ST), EC, CA1, hilus, granular layer, sub-granular zone (SGZ) and molecular layer of dentate gyrus (DG)] was stained (3× sections in total). Sections were blocked in 1% milk powder, 2% bovine serum albumin (BSA), 0.3% Triton X-II, 1.5% normal goat serum (Chemicon®) or 5% normal donkey serum (Sigma-Aldrich) for 1 h at room temperature (RT), rocking. Followed by 3 × 5 min PBS washes, sections were incubated in primary antibody, diluted in PBS containing 2% BSA, 0.3% Triton X-II, 1.5% normal goat serum or 5% normal donkey serum to working concentrations (Supplementary Table 1) overnight at 4°C, and the following day for 1 h at RT. Sections were washed (3 × 5 min, PBS) before incubation (1 h, RT) with secondary antibody, containing 2% BSA and PBS, diluted to working concentrations. Serial sections were mounted onto slides (VWR® SuperFrost Microscope Slides, 1-mm thick; Borosilicate glass coverslips, 22 mm × 50 mm, VWR®

International), using ProLong Gold Antifade Mountant with 4′,6-diamidino-2-phenylindole (Thermo Fisher Scientific, UK) for nuclear staining.

HRP-enhanced immunohistochemistry of ChAT and p75^{NTR} (Warsaw)

Female, homozygous L1, L66 and WT (NMRI) mice at 3 and 9 months were terminally anaesthetized with pentobarbital (Morbital; 1.7 ml/kg) by intraperitoneal injection. Mice were subsequently perfused with 0.01 M PBSV with 0.05% heparin (w/v) and then with 4% paraformaldehyde containing 15% saturated picric acid for fixation and cryopreserved in 5% glycerol/2% DMSO (0.1 M PBSV, pH = 7.4). Whole brains were dissected and post-fixed in 4% paraformaldehyde (12 h), followed by a 24 h incubation in 10% glycerol/2% DMSO (0.1 M PBS, pH = 7.4; 1 mM Na$_3$VO$_4$; PBSV) and 20% glycerol/2% DMSO (PBSV), over 3 days. After post-fixation, brains were snap-frozen on dry ice and stored in −80°C until staining. Whole brains were embedded in Shandon^{TM} Cryomatrix^{TM} embedding resin (Thermo Fisher Scientific, USA) and sectioned at 40 µm. Free-floating sections were washed in 0.1 M PBSV (3 × 5 min) and incubated with 1% H$_2$O$_2$ (Chempur, Poland) for 30 min to block endogenous peroxidases. Sections were blocked in a serum solution [5% normal rabbit serum (Vector Laboratories, USA) or 5% normal goat serum (Vector Laboratories, USA) (for ChAT and p75^{NTR}, respectively), 0.3% Triton X-100 (Sigma-Aldrich, USA) in 0.1 M PBSV]. They were then incubated in primary antibody (Supplementary Table 1) in blocking solution (1% BSA) for 1 h at RT, and overnight at 4°C. Sections were washed in PBSV (3 × 5 min) before incubation with secondary antibody (0.1 M PBSV with 5% normal rabbit serum/5% normal goat serum, 1% BSA, 0.3% Triton X-100), diluted to working concentrations (Supplementary Table 1) for 1 h at RT. Sections were washed (PBSV, 3 × 5 min) and incubated with horseradish peroxidase-conjugated streptavidin, 1% BSA, and PBSV (1:500; Vector Laboratories Inc.). Following 3 × 5 min PBSV washes, sections were finally incubated with 3,3′-diaminobenzidine (0.025%) in 0.1 M PBSV containing 0.04% NiSO$_4$ and 0.025% H$_2$O$_2$. The reaction was stopped via the addition of 0.1 M PB (pH 7.4). After 3 × 5 min washes (0.1 M PB), sections were mounted onto glass slides, allowed to dry, before immersion in xylene, and mounted in DePeX.

Enzyme-linked immunosorbent assay of IL-1β and C3

Adult female homozygous 6-month-old L1, L66 Tg mice and WT NMRI mice were decapitated and the ST (with nucleus accumbens) and hippocampus collected and stored at −80°C, until further use. Concentrations of IL-1β ($n = 3$) and complement 3 (C3, $n = 5$) were quantified by enzyme-linked immunosorbent assay in regions of interest (Mouse Interleukin 1beta ELISA Kit,

MyBioSource, USA; Mouse Complement Component 3 ELISA Kit, MyBioSource, USA), according to manufacturer's instructions, and results expressed in pictograms per millilitre and micrograms per millilitre, respectively. All standards and samples were added in duplicate to the microtiter plate, and the IL-1β and C3 concentrations were calculated from standard curves.

AChE histochemistry

In accordance with a modified version of Koelle–Friedenwald method (Koelle and Friedenwald, 1949), air-dried sections on glass slides were rinsed in double-distilled water and, to reveal hippocampal or cortex staining, incubated for 1 or 1.5 h, respectively, at RT, shaking, in solution (ethopropazine, glycine, $CuSO_4 \cdot 5H_2O$, acetylthiocholine iodide, sodium acetate, glacial acetic acid, double-distilled water). Slides were washed 6×5 min with water and developed (1.25% sodium sulphide solution) for 1 min. Slides were washed again for 6×5 min with water and incubated with intensifying solution (1% $AgNO_3$, w/v) in water, washed 3×5 min with water and incubated again for 2×5 min (5% $Na_2S_2O_3$, w/v), at RT with shaking. Finally, slides were washed 6×5 min with water before immersion in xylene and mounted in DePeX.

Quantitative analysis of ChAT, Iba1 and GFAP-IR neurons (Aberdeen)

Fluorescent images of ChAT, Iba1 and GFAP-IR were obtained under a Zeiss-Axio Imager M1 upright fluorescence microscope (Zeiss, Germany). Stereological cell counting of ChAT-stained neurons was recorded using the Optical Fractionator method of Stereo Investigator Stereology Software (MBF Bioscience). Regions were identified microscopically in accordance with the Mouse Brain Stereotaxic Atlas (Paxinos and Franklin, 2012) as MS, nBM the VDB and HDB, the nucleus basalis magnocellularis (nBM), ST and EC. Hippocampal regions were identified as the sub-regions of the DG: hilus, granular layer, SGZ molecular layer and as CA1 (see Supplementary Fig. 1). A cell was considered as a cholinergic neuron when the following criteria were reached: ChAT immunoreactivity of neuronal somata as well as good visibility of cell nucleus and proximal segment of two or more dendrites within the counting frame, allowing for the exclusion of neuronal debris. Regions were outlined using a 2.5× magnification, and cell counting was carried out using the 20× magnification by an experienced experimenter. There was no sample blinding.

Quantitative analysis of ChAT-IR neurons (Warsaw)

Sections were imaged under a Nikon Eclipse Ni-E microscope. The computerized densitometric image analysis (NIS-Elements BR4.30.00; Nikon Instruments) of ChAT-IR neurons was performed in the basal forebrain regions (MS, VDB, HDB, nBM and ST). Regions were identified microscopically in accordance with the Mouse Brain Stereotaxic Atlas (Paxinos and Franklin, 2012). Regions of interest were outlined using the software's X–Y plotting system that measures the square area (mm^2) of the marked frame, and ChAT-IR neurons were counted manually at 400× magnification. Cell counts per section were then corrected with the Abercrombie's formula (Abercrombie, 1946), and the packing density of the cholinergic neurons was calculated as a function of rostro-caudal level and location within the studied structures by using the obtained cell counts and the square area of the marked frames in each analysed section. Therefore, the mean number of ChAT-IR neurons obtained from each experimental group was expressed as packing density (the number of cells/mm^2).

Quantitative analysis of AChE

AChE was analysed microscopically at 100× magnification using NIS-Elements BR4.30.00 Software. Measurements were taken from a fixed area of $75\,000 \pm 500$ mm^2 in the primary somatosensory cortex and the CA3 hippocampal area, which comprises a cross-section of all cortical or hippocampal layers. Data are presented as the mean optical density in Tg L1 or L66 (for both lines $n = 3$) or WT mice ($n = 2$) at 3 and 12 months of age.

Statistical analysis

All data sets are expressed as group mean $\pm$ SEM for the number of experiments indicated in the figure and table legends. Data were analysed using one-way or two-way ANOVA, followed by *post hoc* comparison using two-tailed Student's *t*-tests and Newman–Keuls test. Specific weight was given to the comparison between Tg and WT mice, but not between Tg lines. The Mann–Whitney *U*-test for independent groups was also used, when appropriate. Differences between groups were considered statistically significant for *$P < 0.05$. Statistical analyses were performed using GraphPad Prism 5.04 (Aberdeen, UK) and STATISTICA 12 software (Warsaw, Poland).

Data availability

All the raw data supporting the results of this study are available at the reader's request.

Results

Loss of cholinergic neurons in the basal forebrain of L1 mice

Immunofluorescence levels of the ChAT enzyme were determined using two independent experiments using two immuno-histochemical staining methods in coronal mouse brain sections of the basal forebrain. Sections from L1
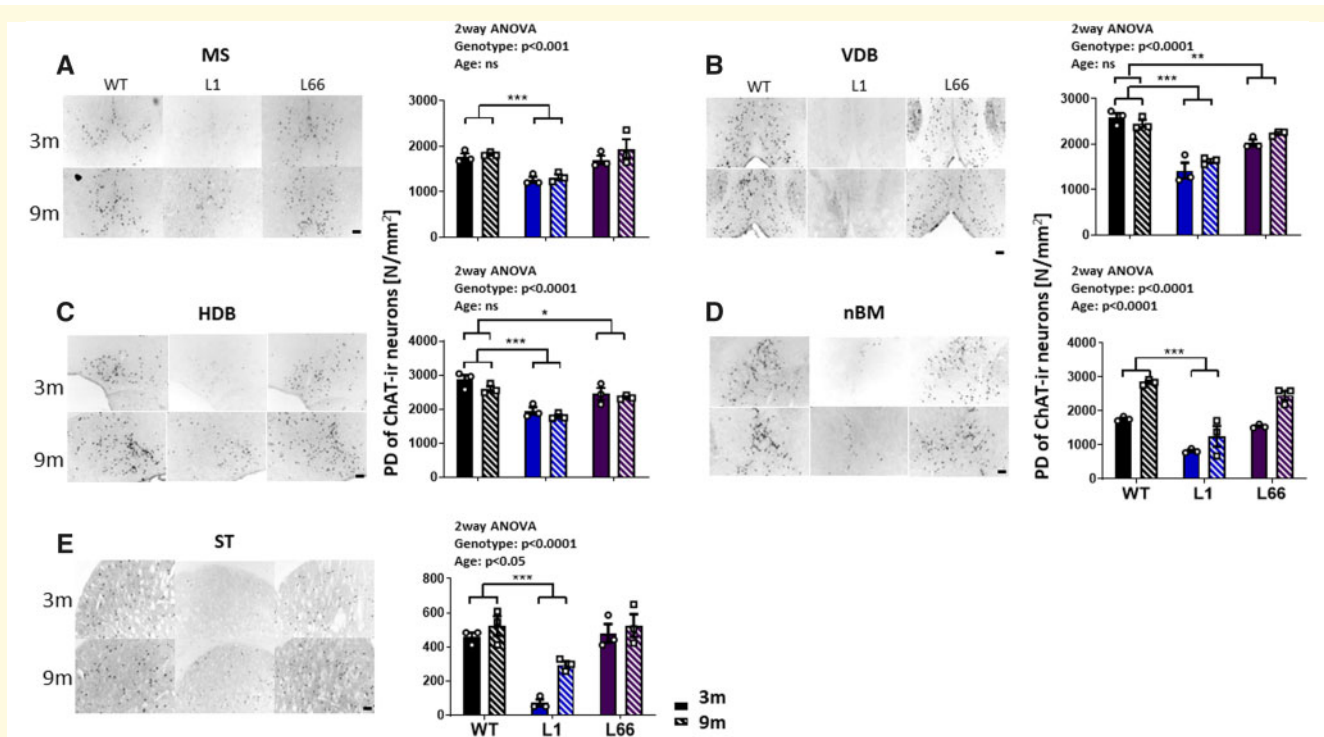
Figure 1 ChAT staining intensity is reduced in L1 basal forebrain at 3 and 9 months. Representative microphotographs and quantification of ChAT immunohistochemical staining in the basal forebrain regions of (**A**) MS, (**B**) VDB, (**C**) HDB, (**D**) nBM and (**E**) ST in 3- and 9-month-old transgenic L1 ($n = 3$), L66 ($n = 3$) and WT (NMRI; $n = 3$) mice. Images were obtained at a $100\times$ magnification. Scale bar: 200 μm. Cell counts are expressed as PD of ChAT-IR neurons (N/mm^2). The effect of genotype was determined using a two-way ANOVA, with transgene and age as factors followed by the Newman–Keuls test. Data were considered statistically significant with alpha set to 5%. *$P < 0.05$, **$P < 0.01$ and ***$P < 0.001$. Data presented as mean ± SEM. PD = packing density; ST = striatum.

animals at 3, 6 and 9 months show a clear reduction in both density and total ChAT-IR neuron cell count in basal forebrain regions of the MS, nBM, VDB, HDB and ST, compared to WT brain sections (Figs 1 and 2). A two-way ANOVA with genotype and age returned a $P < 0.001$ for the factor genotype in all regional comparisons. This effect was mainly due to significantly reduced ChAT-IR packing densities in basal forebrain and ST of L1 (Fig. 1A–E, MS, VDB, HDB, nBM and ST; all P-values < 0.001 compared with WT). In addition, the age factor was significant only in nBM ($P < 0.0001$) and in ST ($P < 0.05$), but not in MS, VDB or HDB.

In agreement with the above profile, an independent set of experiments using fluorescence measured total ChAT cell counts in L1 and L66 at 6 months of age. It confirmed reduction in ChAT positivity in L1 for all regions of the basal forebrain, but not in L66. The reduction for all regions was between 30% (MS) and 60% (nBM) in L1 compared to WT (Fig. 2A–E, Supplementary Table 2).

Altered AChE in cortex and hippocampus of L1 mice

The AChE activity was assessed histochemically from an area cross-sectioning through all cortical and hippocampal layers. The staining was visibly weaker in L1 mice compared with WT at 3 and 12 months (Fig. 3). Densely stained individual cortical layers could not be distinguished in L1 tissue, whereas WT and L66 exhibited two distinct bands with high staining intensity corresponding with cortical layers II and V. This was confirmed quantitatively (Fig. 3C and D). There was also a significant decrease in AChE staining within cortex of L1 mice compared with age-matched WT ($P < 0.001$; Fig. 3C).

AChE staining in hippocampus was lower in L1 relative to WT ($P < 0.001$) (Fig. 3D). Conversely, increased AChE staining intensity was observed in L66 relative to WT ($P < 0.01$) probably due to the elevated AChE level in 3-month L66 mice as compared to age-matched WT. Moreover, L1 and L66 mice displayed a significant decrease in AChE staining with age (age factor $P < 0.05$) (Fig. 3D).

Decreased low-affinity neurotrophin receptor staining in L1 basal forebrain

The qualitative immune-histochemical examination of low-affinity neurotrophin receptor showed a decrease in both the number of p75^{NTR}-IR neurons and the intensity of staining in L1 mice in MS, VDB, HDB and nBM in
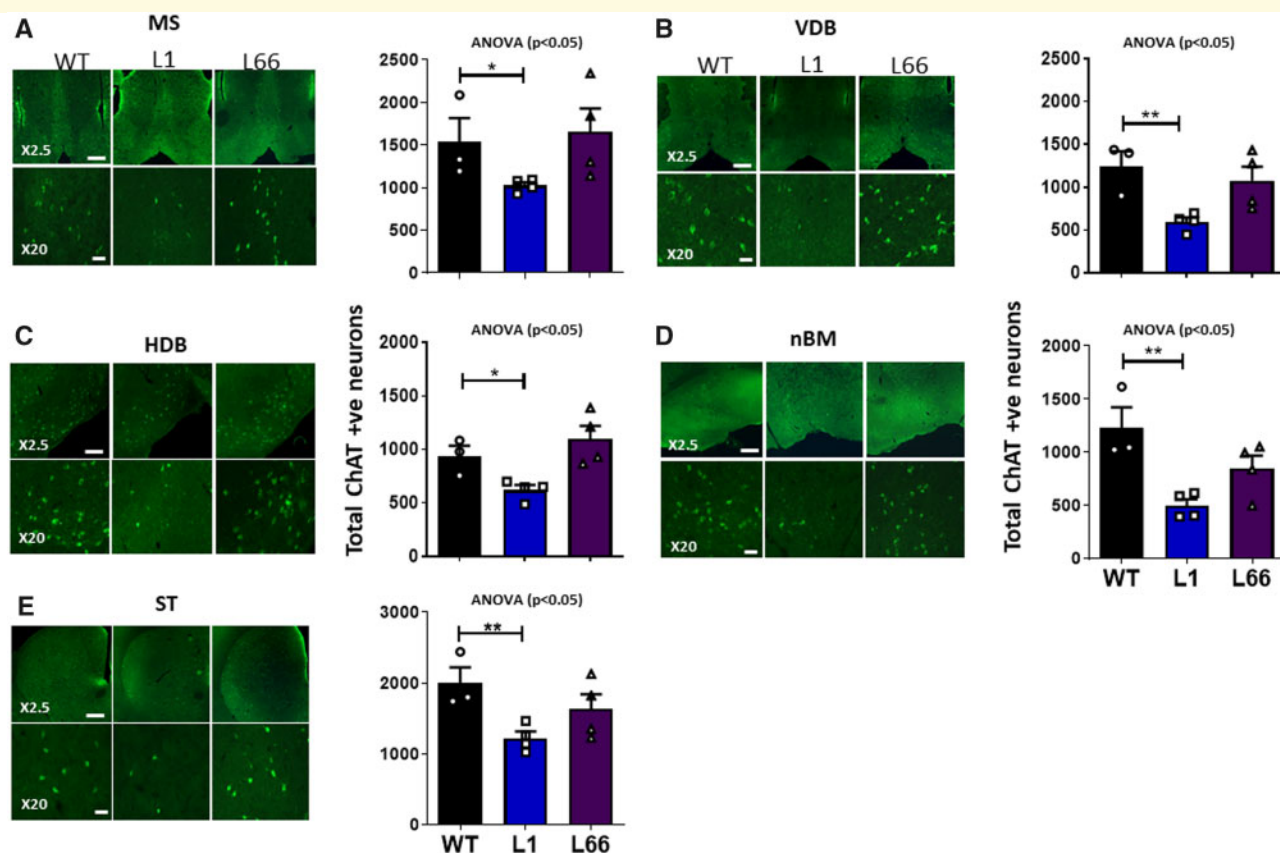
Figure 2 ChAT staining intensity is reduced in L1 basal forebrain at 6 months. Fluorescence microscopic images of ChAT expression and ChAT stereological cell counting from basal forebrain regions of the (**A**) MS, (**B**) VDB, (**C**) HDB, (**D**) nBM and (**E**) ST in L1 ($n = 4$), L66 ($n = 4$) and WT (NMRI, $n = 3$) mice. Representative images were obtained at $2.5\times$ or $20\times$ magnification, as indicated. Scale bar $2.5\times$, 450 μm; $20\times$, 55 μm. Cell counts are expressed as total cells. The effect of genotype was determined using a one-way ANOVA and individual genotype differences by Student's t-test. Data were considered statistically significant when $*P < 0.05$ and $**P < 0.01$. Data presented as mean ± SEM. ST = striatum.

comparison to WT (Fig. 4A–D). This was already present at 3 months of age, and there was a further decline in mice at 9 months. In contrast, the p75[NTR] staining of 3-month-old L66 mice showed a positive p75[NTR]-immunoreactivity resembling the pattern in WT, with particularly strong staining in cell bodies and neuropil. In addition, at 9 months, the intensity of p75[NTR] staining did not seem to be altered in L66 or WT (Fig. 4).

The quantitative analysis revealed decreased packing density of p75[NTR] in L1 mice as compared to WT in all studied structures (MS, $P < 0.001$; VDB, $P < 0.001$; HDB, $P < 0.001$; nBM, $P < 0.001$). In turn, age factor reached significance only in nBM. In 9-month-old animals of all groups, p75[NTR] packing density was elevated as compared to 3 month-old mice and resembled the pattern seen in ChAT staining.

Increased glial staining in both L1 and L66 basal forebrain

To gain further insight into the neuroinflammatory profile induced by tau overexpression in our Tg models, an analysis of Iba1 and GFAP-IR was conducted using immune-histochemical fluorescence staining methods. An initial focus was placed on the basal forebrain regions, for which a selective decline in ChAT positivity had been confirmed (see Figs 1 and 2). Areas included MS, nBM, VDB, HDB and ST.

A significant increase in the density of Iba1-IR was observed in L1 in VDB and HDB ($P < 0.01$) and ST ($P < 0.05$; Fig. 5B, C and E) at 6 months. The HDB was the only basal forebrain region, in which a significant increase in GFAP-IR was seen in L1 ($P < 0.05$, Fig. 6C, Supplementary Table 2). A robust increase in Iba1-positive microglia in L66 animals was observed for all basal forebrain regions apart from the nBM ($P < 0.01$; Fig. 5A–C and E). In parallel with L1, L66 also displayed a significant increase ($P < 0.01$) in the density of GFAP-reactive astrocytes within the HDB (Fig. 6, Supplementary Table 2). It is intriguing to note that, despite the robust cholinergic loss of ChAT in nBM of L1 animals (Figs 1 and 2; Supplementary Table 2), this was not matched by enhanced inflammatory responses of either Iba1 or GFAP.
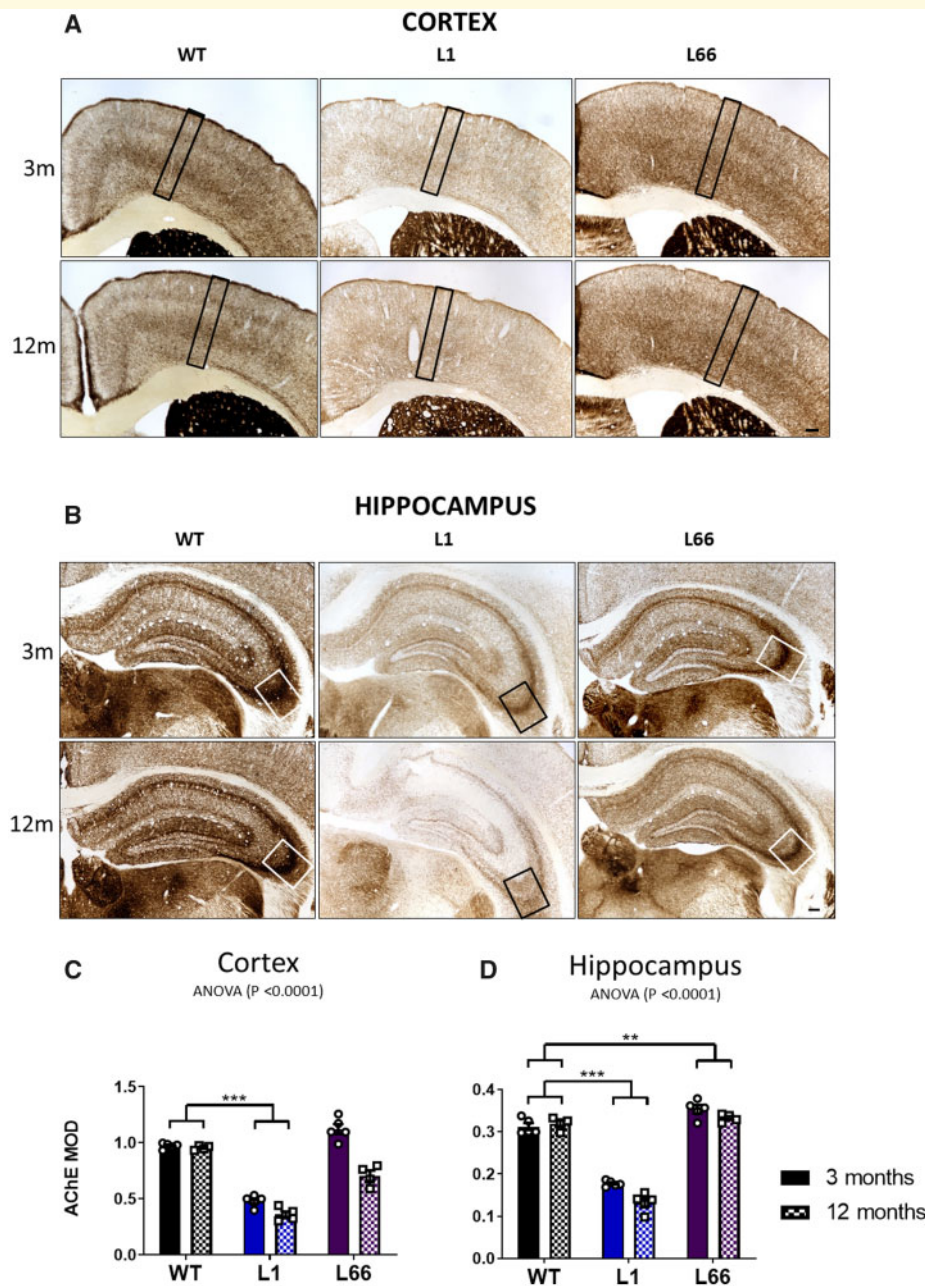
Figure 3 Intensity of AChE staining is reduced in L1 cortex and hippocampus. Representative microphotographs of AChE MOD in cortex (**A**) and hippocampus (**B**) of transgenic L1, L66 and WT (NMRI) mice at 3 and 12 months. $n = 5$ for all groups except WT, L66 cortex at 12 months, and WT, L66 hippocampus at 12 months, where $n = 4$ per group. The rectangle represents the area of measurement for the analysis of MOD in the cortex and hippocampus. Scale bar: 100 μm. MOD of AChE quantified in cortex (**C**) and hippocampus (**D**) of transgenic L1, L66 and WT (NMRI) mice at 3 and 12 months. The AChE is presented as MOD + SEM. Main effects were determined using two-way ANOVA and the source of significance explored by *post hoc* Newman–Keuls test. Data were considered statistically significant with alpha set to 5%. *$P < 0.05$, **$P < 0.01$ and ***$P < 0.001$. Data presented as mean ± SEM. MOD = mean optical density.

Increased glial immunostaining in hippocampal sub-regions of both L1 and L66

To evaluate the microglial and astrocyte contribution to the disease pathogenesis induced by ChAT loss and tau overexpression in Tg models L1 and L66, immunohistochemical fluorescence staining methods were used on coronal mouse brain sections of the DG (hilus, molecular layer, granular layer, SGZ), hippocampus and EC. Representative images displaying selected brain regions for Iba1 and GFAP-IR counting in the hippocampus proper and DG micro-circuits are given in Fig. 7A and Supplementary Fig. 1. Robust microgliosis based on a significant increase in Iba1-IR
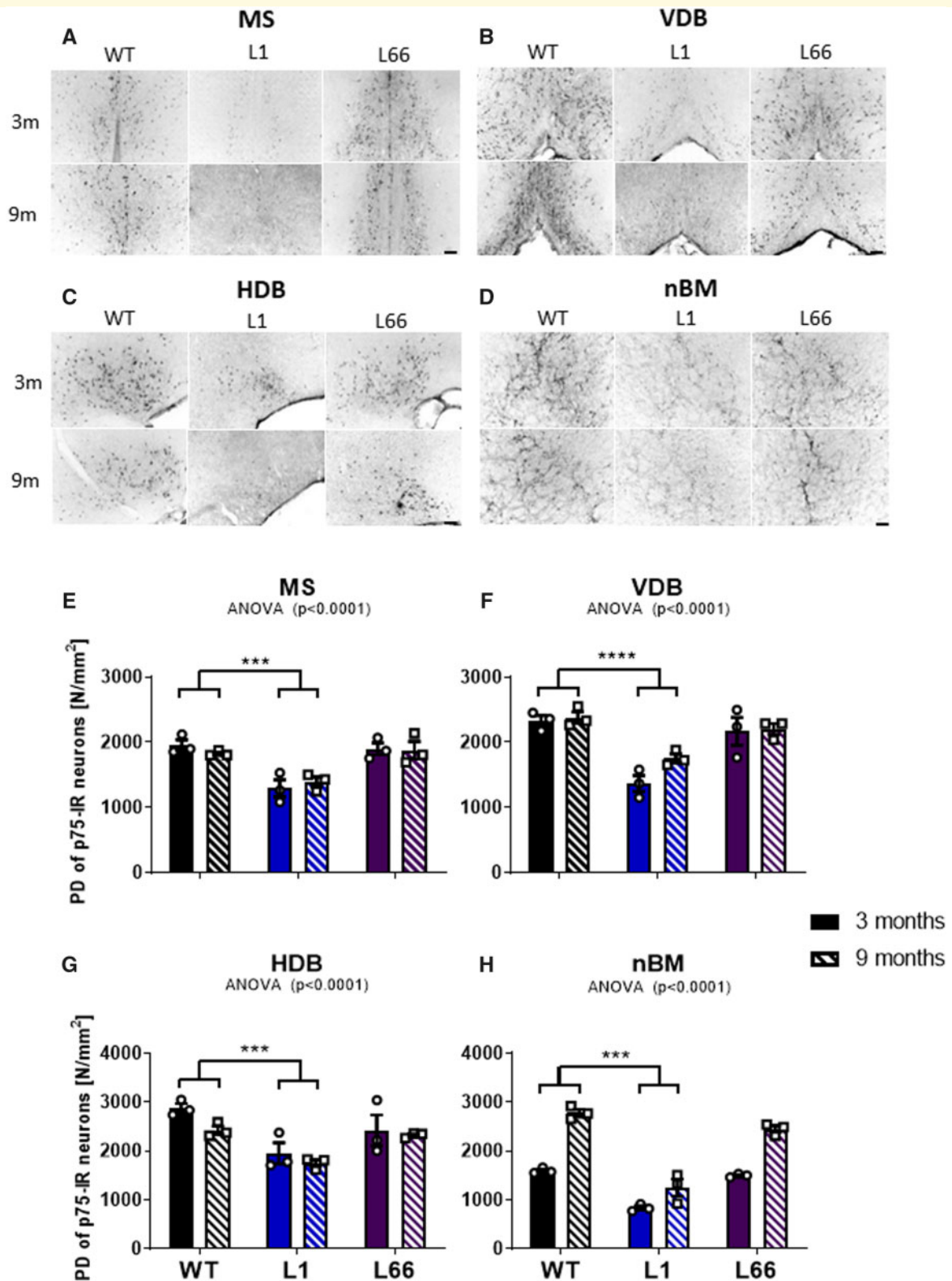
Figure 4 p75^{NTR} immunohistochemistry in L1 and L66 basal forebrain. Representative microscopic images of p75^{NTR} immunohistochemical staining and PD of p75-IR neurons (N/mm^2) in the basal forebrain regions of (**A, E**) MS, (**B, F**) VDB, (**C, G**) HDB and (**D, H**) nBM in 3- and 9-month-old transgenic L1 ($n = 3$) and L66 ($n = 3$) and WT NMRI ($n = 3$) mice. Images were obtained at a $100\times$ magnification. Scale bar represents 200 μm. The effect of genotype was determined using a two-way ANOVA, with transgene and age as factors followed by Newman–Keuls test. Data were considered statistically significant with alpha set to 5%. *$P < 0.05$, **$P < 0.01$ and ***$P < 0.001$. Data presented as mean ± SEM. PD = packing density.
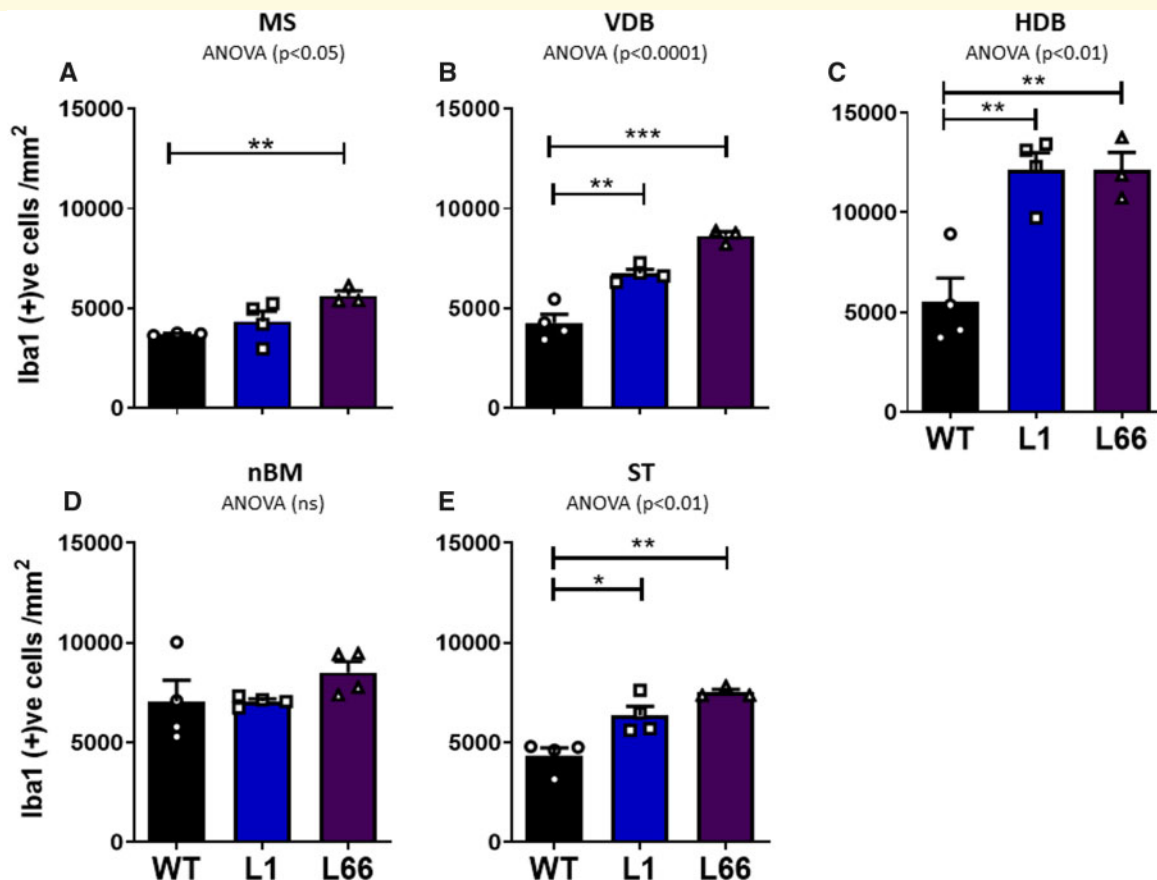
Figure 5 Increased microglia in L1 and L66 mice. Iba1 stereological cell-counting analysis from basal forebrain regions of the (**A**) MS, (**B**) VDB, (**C**) HDB, (**D**) nBM and (**E**) ST in transgenic L1 ($n = 4$), L66 ($n = 4$) and WT (NMRI, $n = 4$) mice at 6 months. Cell counts are expressed as the density of Iba1-positive cells (cells/mm^2). Main effects of genotype were determined by one-way ANOVA, and the source of reliability was confirmed by *post hoc* Student's *t*-test. Data were considered statistically significant when *$P < 0.05$, **$P < 0.01$ and ***$P < 0.001$. Data presented as mean ± SEM. ST = striatum.

density was observed in L1 mice and this was specific to the SGZ of the DG (SGZ $P < 0.001$; Fig. 7A, G, H) and the EC ($P < 0.05$; Fig. 7C and I). In L66, microgliosis was more widespread and heightened Iba1 reactivity was observed in the hilus of the DG, granular layer, SGZ (all P's < 0.001), and the EC ($P < 0.01$), relative to WT mice (Fig. 7A, C-G, I).

No gliosis was observed in the molecular layer of the dentate or CA1 in either Tg line confirming the specificity of inflammatory responses to sub-regions. As for GFAP-IR astrocyte activation, there was a significantly increased density specific to the SGZ in L1 and L66 ($P < 0.05$), but not for other areas of the hippocampus (Fig. 7B, H, J, Supplementary Table 2).

Increased concentrations of IL-1β and C3 in the hippocampus of L1 and L66 mice

Quantitative analysis of complement C3 and IL-1β was measured in ST with nucleus accumbens and

hippocampus from 6-month-old Tg L1, L66 and WT (NMRI) mice (Fig. 8). In the ST, there was no difference in IL-1β and C3 concentrations between NMRI, L1 and L66 mice (Fig. 8A and C).

In the hippocampus, statistical analysis showed significantly higher concentrations of IL-1β and C3 in L1 ($P < 0.01$ for IL-1β and C3) and L66 mice ($P < 0.05$ for IL-1β and $P < 0.01$ for C3) compared to NMRI controls (Fig. 8B and D).

Discussion

We report here on the distinct cholinergic and inflammatory phenotypes in the tau Tg mouse models L1 and L66, observations which permit a strong discrimination between Alzheimer's disease-like and FTLD-like pathology in these mice. These models overexpress two different tau protein species: truncated paired helical filament-core tau (L1) and full-length mutant tau (L66) expressed under the pan neuronal-specific Thy1 promoter. In addition, it
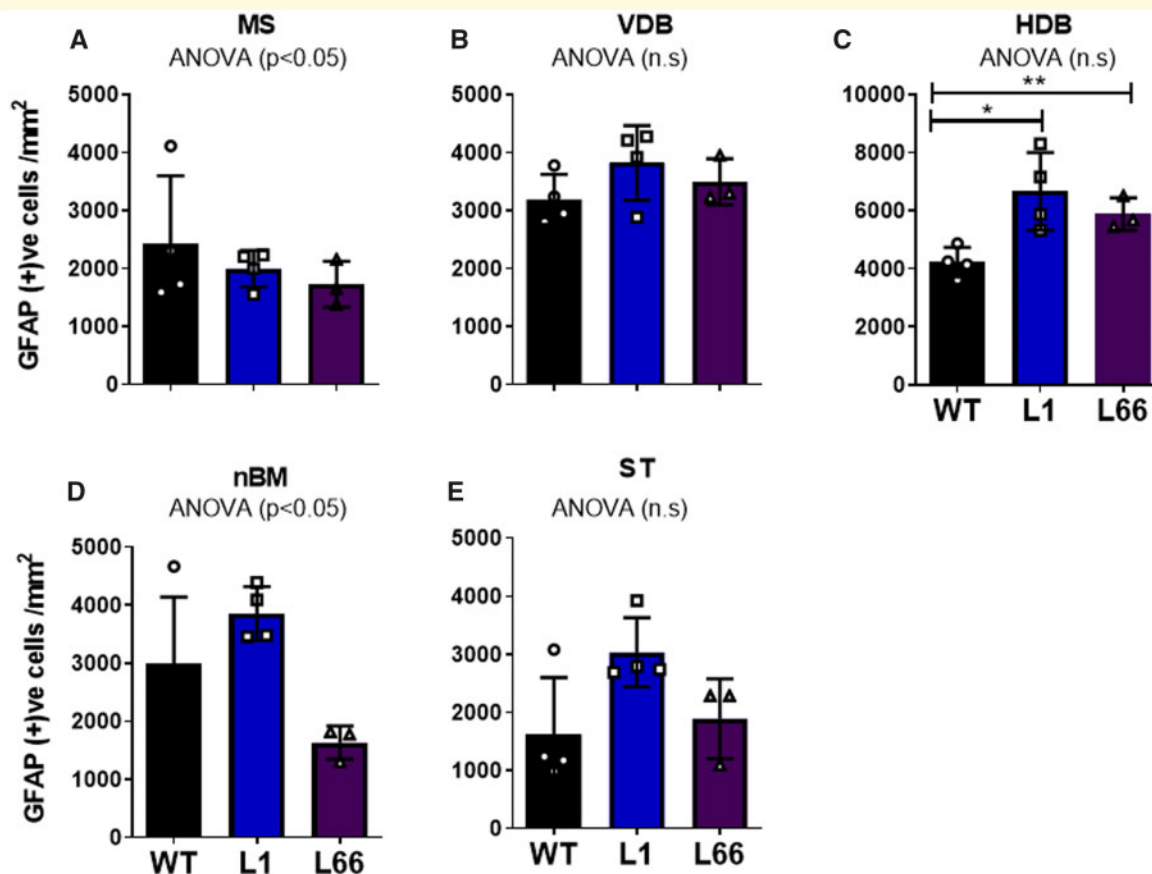
Figure 6 Basal forebrain gliosis in both transgenic models. GFAP stereological cell-counting analysis from basal forebrain regions of the **(A)** MS, **(B)** VDB, **(C)** HDB and **(D)** nBM; **(E)** ST, in transgenic L1 ($n = 4$), L66 ($n = 4$) and WT (NMRI, $n = 4$) mice at 6 months. Cell counts are expressed as the density of GFAP-positive cells (cells/mm^2). Main effects of genotype were determined by one-way ANOVA, and the source of reliability was confirmed by *post hoc* Student's *t*-test. Data were considered statistically significant when *$P < 0.05$, **$P < 0.01$ and ***$P < 0.001$. Data presented as mean $\pm$ SEM. ST = striatum.

must be mentioned that L66 has an additional endoplasmic reticulum targeting signal sequence peptide, which is lacking in L1 mice (Melis *et al*, 2015a), albeit this is unlikely to have any influence on the following phenotypes reported in this study. Pathologically, mice mimic an Alzheimer's disease-like pathology that follows a Braak-like progression (Braak and Braak, 1995) and features cognitive impairment (Melis *et al.*, 2015). L66 mice mimic FTLD-like pathology and feature an early-onset motor deficit that becomes more severe with age (Melis *et al.*, 2015).

L1 exhibits features of Alzheimer's disease

In the basal forebrain of L1, we observed a significant loss of cholinergic neurons at 3, 6 and 9 months, compared to control groups, in two independently conducted studies. Lack of reproducibility between rodent pathological pre-clinical studies is a prevalent issue (Treuting *et al.*, 2016; Ward *et al.*, 2017). Therefore, these two

independent, parallel studies robustly support this cholinergic phenotype observed in L1 and lack thereof in L66.

In agreement with the Alzheimer's disease-like phenotype of L1, the significant basal forebrain cholinergic neuron loss matches that observed in post-mortem brains of patients with Alzheimer's disease (Davies and Maloney, 1976; Whitehouse *et al.*, 1982). Cholinergic afferents of the MS and VDB project towards the hippocampus via the septo-hippocampal pathway, and cholinergic somata in the nBM primarily target the cortical neurons via the baso-cortical pathways (Khakpai *et al.*, 2013). Specifically, cholinergic afferents from the MS to hippocampus appear crucial in the regulation of spatial and mnemonic function (Okada *et al.*, 2015). A lowering in basal forebrain cholinergic ChAT-IR neurons would therefore contribute to an explanation of the behavioural age-dependent deficits in episodic-like memory previously observed in L1 (Melis *et al.*, 2015) and is at the same time reminiscent of the pathology and cognitive decline typically at play in Alzheimer's disease (Grothe *et al.*, 2010; Pedroso *et al.*, 2018).
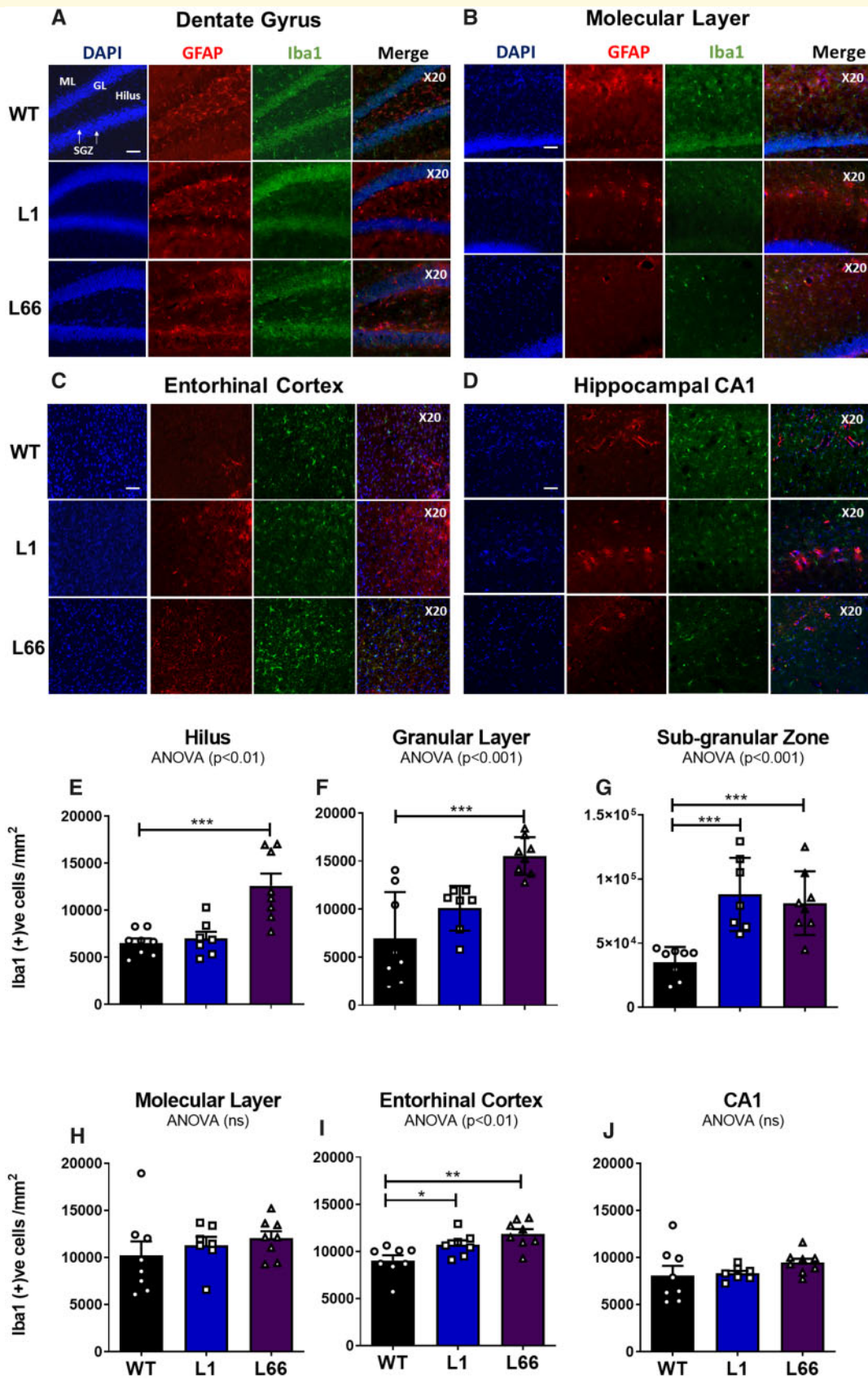
Figure 7 Hippocampal neuroinflammation in L1 and L66 mice. Representative fluorescence images for double labelling of microglia and astrocytes (**A–D**). Thirty micrometre sections are stained for Iba1 (green), GFAP (red) and 4′,6-diamidino-2-phenylindole (blue) for selected dentate gyrus sub-regions of the hilus, sub-granular zone, molecular layer, granular layer, hippocampal CA1 region and entorhinal cortex in WT
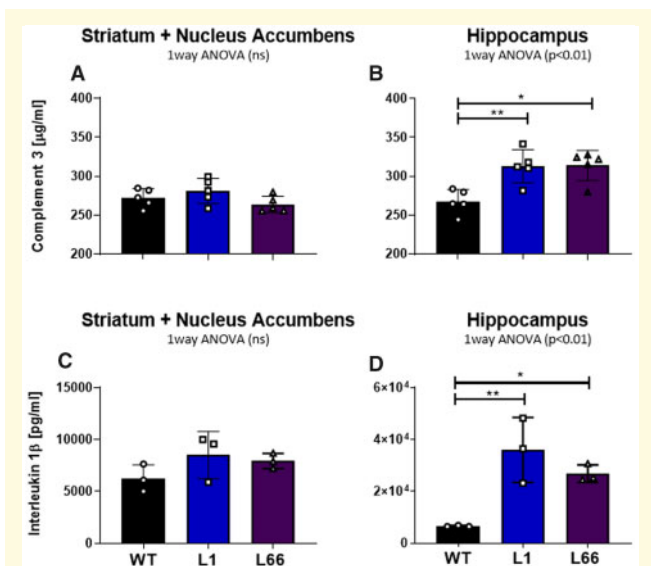
Figure 8 Quantitative analysis of complement C3 in striatum with nucleus accumbens (**A**), hippocampus (**B**) and interleukin 1β (**C, D**) from 6-month-old transgenic L1, L66 and WT (NMRI) mice at 6 months. For all genotypes, $n = 3$ for striatum and $n = 5$ for hippocampus. Concentrations were measured by enzyme-linked immunosorbent assay. Data are presented as mean $\pm$ SEM. Interactions between groups were determined using one-way ANOVA and the source of significance explored by *post hoc* Newman–Keuls test. **$P < 0.01$. Data presented as mean $\pm$ SEM.

A reduction in striatal ChAT was also observed in L1 at 3, 6 and 9 months, data that match that of the human Alzheimer's disease brain, where there is a reduction in ChAT in the ventral and dorsal ST (Boissière *et al.*, 1997). In addition, a significant reduction in AChE staining intensity was observed in both cortex and hippocampus of L1 at 3 and 12 months.

In line with the ChAT reduction in L1, hippocampal AChE levels have been reported to be significantly reduced in patients with mild cognitive impairment and early Alzheimer's disease (Rinne *et al.*, 2003), displaying robust correlations to cognitive impairment (Shinotoh *et al.*, 2000; Bohnen *et al.*, 2005). Given the cognitive phenotype in L1 (Melis *et al.*, 2015), the observed reduction in AChE levels may explain some of the spatial learning and memory deficits known for L1 mice.

Survival of basal forebrain cholinergic neurons is entirely dependent on the binding of nerve growth factor to hippocampal and cortical receptors including tropomyosin receptor kinase A and p75[NTR] (Niewiadomska *et al.*, 2011). An age-dependent reduction in p75[NTR] was observed in L1 from 3 months onwards in basal forebrain regions of the MS, VDB, HDB and nBM. These parallel post-mortem observations in patients with Alzheimer's disease, in which p75[NTR] is significantly reduced in the nucleus basalis of Meynert, the equivalent of the murine nBM (Salehi *et al.*, 2000; Mufson *et al.*, 2002). However, no age-dependent reduction in ChAT was observed in L1 mice suggesting that ChAT reduction occurs early on and this pathology remains steady with age.

At the same time, an increase in microglial activation in the basal forebrain of L1 mice may also be initiated by a ChAT reduction at 6 months or earlier. Equivalent studies in rodent models have shown that selective lesioning of the basal forebrain leads to a direct increase in susceptibility to cognitive deficits induced by acute inflammation (Field *et al*, 2012); therefore, this increase in microglial activation may also contribute to an explanation of the cognitive deficits observed in L1 at 3 months of age (Melis *et al.*, 2015). Enhanced neuroinflammation was confirmed in L1 as a significant increase in the expression of Iba1 in the VDB, HDB and ST. Our data suggest that microglial activation in L1 may follow a cholinergic loss in corresponding basal forebrain regions, albeit microglial activation was observed at 6 months only, and was not investigated at 3 months in this study. However, this could suggest a potential predisposition of regions affected by cholinergic neuron loss, as being susceptible to microglial recruitment and activation.

This hypothesis has been explored previously in mice, where pre-existing cholinergic deficits can result in a predisposition towards inflammatory insult, through up-regulation of inflammatory markers IL-1β, tumour necrosis factor alpha and IL-6, following selective basal forebrain lesioning (Field *et al.*, 2012). A significant increase in microglial marker Iba1 was observed across hippocampus, EC, of L1 mice. Of note is the particularly high expression of microglia in the SGZ, as this specific area of the DG is where neurogenesis primarily occurs (van Praag *et al.*, 2002). Previous studies have suggested that a disruption in neurogenesis, particularly through neuroproliferation observed in the DG, may be potentially associated with the age-dependent decrease in hippocampal learning and memory in Alzheimer's disease (Jin *et al.*, 2004). Specifically, microglia and astrocytes

Figure 7 Continued
mice AT 6 months. Representative images were obtained at 20× magnification. Scale bar, 55 μm. (E–J) Quantification of Iba1 stereological cell counting from dentate gyrus and hippocampal regions from transgenic L1 ($n = 7$), L66 ($n = 8$) and WT (NMRI, $n = 8$) mice at 6 months. Cell counts are expressed as Iba1-positive cells (cells/mm²). Quantification of GFAP stereological cell counts is found in Supplementary Fig. 2. Main effects of genotype for each area were determined using one-way ANOVA, and the source of significance was traced by *post hoc* Student's *t*-tests. Data were considered statistically significant when *$P < 0.05$, **$P < 0.01$ and ***$P < 0.001$. Data presented as mean $\pm$ SEM. DAPI = 4′,6-diamidino-2-phenylindole.

influence neurogenesis through the induction of apoptosis and the negative regulation of neurogenesis via Notch-mediated signalling pathways (Sierra *et al.*, 2010; Wilhelmsson *et al.*, 2012). Although not established in this study, it is conceivable that both microglia and astrocyte activation will compromise neurogenesis, thereby explaining some of the cognitive deficits observed in L1/L66 from 3 months of age (Melis *et al.*, 2015a). In addition, a significant increase in IL-1β, a marker of activated microglia, was observed in the hippocampus of L1 mice at 6 months. Heightened expression of pro-inflammatory cytokines, such as IL-1β, has been associated previously with mild cognitive impairment in the brains of patients with Alzheimer's disease (Forlenza *et al.*, 2009). This may be a therapeutic target as the reduction in IL-Iβ attenuated tau pathology in 3×Tg-AD mice (Kitazawa *et al.*, 2011).

Less overlap was observed between the loss of acetylcholine in hippocampus and gliosis. Since cholinergic afferents from the basal forebrain project directly to the hippocampus (Perez-Lloret and Barrantes, 2016), loss of cholinergic labelling in basal forebrain neurons was expected to evoke a secondary inflammatory response in the hippocampus in L1, but not necessarily in L66. The fact that L66 has no cholinergic phenotype in the MS, but expressed strong astrogliosis in the hippocampus, is therefore intriguing. Previously, it has been shown that hippocampal astrocytes respond to acetylcholine released from synaptic terminals, suggesting the possible existence of cholinergic synapse–astrocyte interactions (Araque *et al.*, 2002). The data reported here seem to suggest a dissociation between cholinergic loss in basal forebrain and inflammatory responses in their target structures. We confirmed that the lack of Iba1 microglial activation does not preclude an up-regulation of other neuroinflammatory markers, especially IL-1β and complement C3.

Previous studies have also shown that levels of microglia are substantially elevated in the brains of ageing rodents, and this elevation is not necessarily associated with a cholinergic deficit, particularly within the MS and VDB (McQuail *et al.*, 2011). Furthermore, no differences in Iba1 or GFAP morphology were observed in either basal forebrain or hippocampus of L1 or L66 mice at 6 months. Overall, this suggests that the cholinergic system and inflammation may coincide for specific basal forebrain regions, but that they do not appear to overlap necessarily in region-specific targets in the above models.

L66 is more FTLD-like

In contrast to L1 mice, L66 exhibited no difference in total ChAT-IR neuron cell count at 3–9 months in the basal forebrain (apart from Broca's band) suggesting relatively intact cholinergic function. This finding supports the proposed FTLD-like phenotype for these mice (Melis *et al.*, 2015) and matches the data from patients with FTLD, in which no significant difference in ChAT

activity, relative to age-matched controls, was reported (Procter *et al.*, 1999; Bowen *et al.*, 2008, Hirano *et al.*, 2010). Second, a significant reduction in cortical AChE was observed as late as 12 months in L66, with no difference observed in the hippocampus at the same age. Again, this is reminiscent of patients with FTLD exhibiting no differences in hippocampal AChE levels (Hirano *et al.*, 2006). Third, no changes in p75^{NTR} staining were observed in L66 models at 3 or 9 months, suggesting that neither neuronal cell loss nor loss of cholinergic function accounts for the motor phenotype or intact spatial learning phenotype previously observed in these mice (Melis *et al.*, 2015). The above findings therefore strongly translate to the disease phenotype of FTLD in L66 mice.

In L66, a robust microglial activation was also observed in basal forebrain and ST. This result is interesting, as none of these regions exhibited any change in cholinergic neuron density through the measurement of ChAT activity. The pathway of inflammation in FTLD is much less understood than in Alzheimer's disease, although studies in patients with FTLD have revealed an increase in pro-inflammatory cytokines including tumour necrosis factor alpha and tumour necrosis factor-β (Sjögren *et al.*, 2004). In the brain of patients with FTLD, microglial activation has been widely observed, using immunohistochemistry, in frontal and temporal cortex (Lant *et al.*, 2014), and in dorsolateral prefrontal cortex and hippocampus (Cagnin *et al.*, 2004).

Our study provides the first indication that microglial activation in tau Tg L66 mice that mimic FTLD may be widespread and related to regions affected by tau deposition, such as frontal cortex, EC and hippocampus (Melis *et al.*, 2015) rather than cholinergic degeneration. Activated microglia could promote pro-inflammatory activation of astrocytes (Lian *et al.*, 2016). Interleukin-1α and IL-1β, microglia-derived acute phase cytokines, and activated astrocytes are known to up-regulate the expression of the astrocyte-derived complement protein C3 (Maranto *et al.*, 2008). These cytokines form complex interactions that may be capable of self-propagation, thus leading to chronic overexpression of glial cytokines with neurodegenerative consequences (Mrak *et al.*, 1995). Self-propagation may be facilitated by means of several reinforcing feedback loops. For instance, microglia express the C3a receptor (Zhang *et al.*, 2014) and their function could be impacted by astrocytic release of C3. Directly activated microglia release IL-1 and stimulate the astrocyte complement system, leading to additional microglial activation through C3a receptors. Thus, a microglial IL-1β-astrocytic C3–microglial C3a receptor positive feedback loop could govern inflammatory dynamics and tau neuropathology. These interactions with tau remain poorly understood, but available data suggest that the severity of both astrogliosis and microglial activation is linked to tau species and to the severity of aggregated tau.

Finally, both L1 and L66 show increased GFAP- and Iba1-IR cells in the basal forebrain HDB and SGZ of the DG. In FTLD, astrocytosis has been reported in the absence of neuronal loss (Broe *et al.*, 2004), whilst astrocytic pathology in Alzheimer's disease is directly associated in regions exhibiting neuronal loss (Forman *et al.*, 2005).

Summary

Collectively, two independent studies have observed significant loss of cholinergic staining in the basal forebrain in L1, whilst there is also a sub-regional microglial activation. These observations may help explain in part the cognitive deficits observed in L1 and confirm the Alzheimer's disease-like phenotype. By contrast, L66 exhibited a relatively intact cholinergic system but presented with a robust and widespread microglial activation uncorrelated with cholinergic pathology.

Given the differences in the human tau species expressed in these two mouse models, the overexpression of two different forms of tau can lead to two very distinct and robust phenotypes that show characteristic features of Alzheimer's disease-like and FTLD-like tauopathies. Not only does L1 mimic an age-dependent, Braak-like spread of tau pathology, it also features a loss of cholinergic function that is characteristic of Alzheimer's disease. This differs from L66, with its more robust and widespread tau pathology with considerably more overlap of inflammation, that make it representative of FTLD.

Supplementary material

Supplementary material is available at *Brain Communications* online.

Acknowledgements

Funding

Competing interests

The authors report no competing interests.

References

Abercrombie M. Estimation of nuclear population from microtome sections. Anat Rec 1946; 94: 239–47.

Alzheimer A. Uber eine eigenartige Erkrankung der Hirnrinde. Allg Z Psychiat 1907; 64: 146–8.

Araque A, Martín ED, Perea G, Arellano JI, Buño W. Synaptically released acetylcholine evokes Ca2+ elevations in astrocytes in hippocampal slices. J Neurosci 2002; 22: 2443–50.

Arends Y, Duyckaerts C, Rozemuller JM, Eikelenboom P, Hauw JJ. Microglia, amyloid and dementia in Alzheimer disease. A correlative study. Neurobiol Aging 2000; 21: 39–47.

Belarbi K, Schindowski K, Burnouf S, Caillierez R, Grosjean M-E, Demeyer D, et al. Early Tau pathology involving the septo-hippocampal pathway in a Tau transgenic model: relevance to Alzheimer's disease. Curr Alzheimer Res 2009; 6: 152–7.

Bohnen NI, Kaufer DI, Hendrickson R, Ivanco LS, Lopresti B, Davis JG, et al. Cognitive correlates of alterations in acetylcholinesterase in Alzheimer's disease. Neurosci Lett 2005; 380: 127–32.

Boissière F, Faucheux B, Agid Y, Hirsch EC. Choline acetyltransferase mRNA expression in the striatal neurons of patients with Alzheimer's disease. Neurosci Lett 1997; 225: 169–72.

Bowen DM, Procter AW, Mann D, Snowden J, Esiri M, Neary D, et al. Imbalance of a serotonergic system in frontotemporal dementia: implication for pharmacotherapy. Psychopharmacology 2008; 196: 603–10.

Braak H, Braak E. Staging of Alzheimer's disease—related neurofibrillary changes. Neurobiol Aging 1995; 16: 271–84.

Broe M, Kroil J, Halliday GM. Astrocytic degeneration relates to the severity of disease in frontotemporal dementia. Brain 2004; 127: 2214–20.

Buee L, Bussiere T, Buee-Scherrer V, Delacourte A, Hof P. Tau protein isoforms, phosphorylation and role in neurodegenerative disorders. Brain Res Rev 2000; 33: 95–130.

Cagnin A, Rossor M, Sampson EL, Mackinnon T, Banati RB. In vivo detection of microglial activation in frontotemporal dementia. Ann Neurol 2004; 56: 894–7.

Caillet-Boudin M, Buée L, Sergeant N, Lefebvre B. Regulation of human *MAPT* gene expression. Mol Neurodegener 2015; 10: 28.

Davies P, Maloney AJ. Selective loss of central cholinergic neurons in Alzheimers disease. Lancet 1976; 308: 1403.

Deiana S, Platt B, Riedel G. The cholinergic system and spatial learning. Behav Brain Res 2011; 221: 389–411.

Ferreira-Vieira T, Guimaraes I, Silva FR, Ribeiro FM. Alzheimer's disease: targeting the cholinergic system. Curr Neuropharmacol 2016; 14: 101–15.

Field RH, Gossen A, Cunningham C. Prior pathology in the basal forebrain cholinergic system predisposes to inflammation induced working memory deficits: reconciling inflammatory and cholinergic hypotheses of delirium. J Neurosci 2012; 32: 6288–94.

Forman MS, Lai D, Zhang B, Dabir DV, Swanson E, Lee VM, et al. Transgenic mouse model of tau pathology in astrocytes leading to nervous system degeneration. J Neurosci 2005; 25: 3539–50.

Forlenza CV, Diniz BS, Talib LL, Mendonça VA, Ojopi EB, Gattaz WF, et al. Increased serum IL-1beta level in Alzheimer's disease and mild cognitive impairment. Dement Geriatr Cogn Disord 2009; 28: 507–12.

Ghosh S, Wu MD, Shaftel SS, Kyrkanides S, LaFerla FM, Olschowka JA, et al. Sustained Interleukin-1β overexpression exacerbates tau pathology despite reduced amyloid burden in an Alzheimer's mouse model. J Neurosci 2013; 33: 5053–64.

Götz J, Chen F, Barmettler R, Nitsch RM. Tau filament formation in transgenic mice expressing P301L tau. J Biol Chem 2001; 276: 529–34.

Grothe M, Zaborszky L, Atienza M, Gil-Neciga E, Rodriguez-Romero R, Teipel SJ, et al. Reduction of basal forebrain cholinergic system parallels cognitive impairment in patients at high risk of developing Alzheimer's disease. Cereb Cortex 2010; 20: 1685–95.

Heneka MT, Kummer MP, Latz E. Innate immune activation in neurodegenerative disease. Nat Rev Immunol 2014; 14: 463–77.

Hirano S, Shinotoh H, Kobayashi T, Tsuboi Y, Wszolek ZK, Aotsuka A, et al. Brain acetylcholinesterase activity in FTDP-17 studied by PET. Neurology 2006; 66: 1276–7.

Hirano S, Shinotoh H, Shimada H, Aotsuka A, Tanaka N, Ota T, et al. Cholinergic imaging in corticobasal syndrome, progressive supranuclear palsy and frontotemporal dementia. Brain 2010; 133: 2058–68.

Hirano S, Shintoh H, Shimada H, Tanaka N, Ota T, Sato K, et al. Age correlates with cortical acetylcholinesterase decline in Alzheimer's disease patients: A PET study. Alzheimers Dement 2012; 8: 531–2.

Ittner A, Ittner LM. Dendritic tau in Alzheimer's disease. Neuron 2018; 99: 13–27.

Janeczek M, Gefen T, Samimi M, Kim G, Weintraub S, Bigio E, et al. Variations in acetylcholinesterase activity within human cortical pyramidal neurons across age and cognitive trajectories. Cereb Cortex 2018; 28: 1329–37.

Jin K, Peel A, Mao X, Xie L, Cottrell B, Henshall D, et al. Increased hippocampal neurogenesis in Alzheimer's disease. Proc Natl Acad Sci USA 2004; 101: 343–7.

Kimura T, Sharma G, Ishiguro K, Hisanaga S. Phospho-Tau bar code: analysis of phosphoisotypes of tau and its application to tauopathy. Front Neurosci 2018; 12: 44.

Kitazawa M, Cheng D, Tsukamoto MR, Koike MA, Wes PD, Vasilevko V, et al. Blocking IL-1 signaling rescues cognition, attenuates tau pathology, and restores neuronal β-catenin pathway function in an Alzheimer's disease model. J Immunol 2011; 187: 6539–49.

Khakpai F, Nasehi M, Haeri-Rohani A, Eidi A, Zarrindast M. Septo-hippocampo-septal loop and memory formation. Basic Clin Neurosci 2013; 4: 5–23.

Koelle GB, Friedenwald JS. A histochemical method for localizing cholinesterase activity. Proc Soc Exp Biol Med 1949; 70: 617–22.

Lant SB, Robinson SC, Thompson JC, Rollinson S, Pickering-Brown S, Snowden JS, et al. Patterns of microglial cell activation in frontotemporal lobar degeneration. Neuropathol Appl Neurobiol 2014; 40: 686–96.

Lian H, Litvinchuk A, Chiang A-A, Aithmitti N, Jankowsky JL, Zheng H. Astrocyte-microglia cross talk through complement activation modulates amyloid pathology in mouse models of Alzheimer's disease. J Neurosci 2016; 36: 577–89.

Litvinchuk A, Wan YW, Cole A, Chen F, Liu Z, Zheng H. The role of complement C3 and C2AR receptor in tau pathology and Alzheimer's disease. Alzheimers Dement 2017; 13: 229.

Maranto J, Rappaport J, Datta PK. Regulation of complement component C3 in astrocytes by IL-1β and morphine. J Neuroimmune Pharmacol 2008; 3: 43–51.

McQuail JA, Riddle DR, Nicolle M. Neuroinflammation not associated with cholinergic degeneration in aged-impaired brain. Neurobiol Aging 2011; 32: 2322–3.

Melis V, Zabke C, Stamer K, Magbagbeolu M, Schwab K, Marschall P, et al. Different pathways of molecular pathophysiology underlie cognitive and motor tauopathy phenotypes in transgenic models for Alzheimer's disease and frontotemporal lobar degeneration. Cell Mol Life Sci 2015; 72: 2199–222.

Morales I, Guzmán-Martínez L, Cerda-Troncoso C, Farias GA, Maccioni RB. Neuroinflammation in the pathogenesis of Alzheimer's disease. A rational framework for the search of novel therapeutic approaches. Front Cell Neurosci 2014; 22: 112.

Morimoto K, Horio J, Satoh H, Sue L, Beach T, Arita S, et al. Expression profiles of cytokines in the brains of Alzheimer's disease (AD) patients, compared to the brains of non-demented patients with and without increasing AD pathology. J Alzheimers Dis 2011; 25: 59–76.

Mrak RE, Sheng JG, Griffin WS. Glial cytokines in Alzheimer's disease: review and pathogenic implications. Hum Pathol 1995; 26: 816–23.

Mufson EJ, Ma SY, Dills J, Cochran EJ, Leurgans S, Wuu J, et al. Loss of basal forebrain P75[NTR] immunoreactivity in subjects with mild cognitive impairment and Alzheimer's disease. J Comp Neurol 2002; 443: 136–53.

Nagai T, McGeer PL, Peng JH, McGeer EG, Dolman CE. Choline acetyltransferase immunohistochemistry in brains of Alzheimer's disease patients and controls. Neurosci Lett 1983; 36: 195–9.

Niewiadomska G, Baksalerska-Pazera M, Riedel G. Cytoskeletal transport in the aging brain: focus on the cholinergic system. Rev Neurosci 2006; 17: 581–618.

Niewiadomska G, Baksalerska-Pazera M, Riedel G. The septo-hippocampal system, learning and recovery of function. Prog Neuropsychopharmacol Biol Psychiatry 2009; 33: 791–805.

Niewiadomska G, Mietelska-Porowska A, Mazurkiewicz M. The cholinergic system, nerve growth factor and the cytoskeleton. Behav Brain Res 2011; 221: 515–28.

Okada K, Nishizawa K, Kobayashi T, Sakata S, Kobayashi K. Distinct roles of basal forebrain cholinergic neurons in spatial and object recognition memory. Sci Rep 2015; 5: 13158.

Paxinos G, Franklin KBJ. The mouse brain in stereotaxic coordinates, 2nd edn. San Diego: Academic Press; 2001.

Paxinos G, Franklin K. Paxinos and Franklin's the mouse brain in stereotaxic coordinates, 4th edn. New York: Academic Press; 2012. p. 1–360.

Pedroso R, Corazza D, Andreatto CCA, da Silva T, Costa J, Santos-Galduróz RF. Cognitive, functional and physical activity impairment in elderly with Alzheimer's disease. Dement Neuropsychol 2018; 12: 28–34.

Perez-Lloret S, Barrantes FJ. Deficits in cholinergic neurotransmission and their clinical correlates in Parkinson's disease. NPJ Parkinsons Dis 2016; 18: 16001.

Perry EK, Curtis M, Dick DJ, Candy JM, Atack JR, Bloxham CA, et al. Cholinergic correlates of cognitive impairment in Parkinson's disease: comparisons with Alzheimer's disease. J Neurol Neurosurg Psychiatry 1985; 48: 413–21.

Procter AW, Qurne M, Francis PT. Neurochemical features of frontotemporal dementia. Dement Geriatr Cogn Disord 1999; 10: 80–4.

Raina P, Santaguida P, Ismaila A, Patterson C, Cowan D, Levine M, et al. Effectiveness of cholinesterase inhibitors and memantine for treating dementia: evidence review for a clinical practice guideline. Ann Intern Med 2008; 148: 379–97.

Rinne JO, Kaasinen V, Järvenpää T, Någren K, Roivainen A, Yu M, et al. Brain acetylcholinesterase activity in mild cognitive impairment and early Alzheimer's disease. J Neurol Neurosurg Psychiatry 2003; 74: 113–5.

Robinson L, Goonawardena AV, Pertwee R, Hampson RE, Platt B, Riedel G. WIN55, 212-2 induced deficits in spatial learning are mediated by cholinergic hypofunction. Behav Brian Res 2010; 208: 584–92.

Roy R, Niccolini F, Pagano G, Politis M. Cholinergic imaging in dementia spectrum disorders. Eur J Nucl Med Mol Imaging 2016; 43: 1376–86.

Salehi A, Ocampo M, Verhaagen J, Swaab DF. P75 neurotrophin receptor in the nucleus basalis of meynert in relation to age, sex, and Alzheimer's disease. Exp Neurol 2000; 161: 245–58.

Schindowski K, Bretteville A, Leroy K, Bégard S, Brion J, Hamdane M, et al. Alzheimer's disease-like tau neuropathology leads to memory deficits and loss of functional synapses in a novel mutated tau transgenic mouse without any motor deficits. Am J Pathol 2006; 169: 599–616.

Shinotoh H, Namba H, Fukushi K, Nagatsuka S-I, Tanaka N, Aotsuka A, et al. Progressive loss of cortical acetylcholinesterase activity in association with cognitive decline in Alzheimer's disease: a positron emission tomography study. Ann Neurol 2000; 48: 194–200.

Sierra A, Encinas JM, Deudero JJP, Chancey JH, Enikolopov G, Overstreet-Wadiche LS, et al. Microglia shape adult hippocampal neurogenesis through apoptosis-coupled phagocytosis. Cell Stem Cell 2010; 7: 483–95.

Sjögren M, Folkesson S, Blennow K, Tarkowski E. Increased intrathecal inflammatory activity in frontotemporal dementia: pathophysiological implications. J Neurol Neurosurg Psychiatry 2004; 75: 1107–11.

Spires-Jones T, Stoothoff WH, de Calignon A, Jones PB, Hyman BT. Tau pathophysiology in neurodegeneration: a tangled issue. Trends Neurosci 2009; 32: 150–9.

Terry AV, Buccafusco JJ. The cholinergic hypothesis of age and Alzheimer's disease-related cognitive deficits: recent challenges and their implications for novel drug development. J Pharmacol Exp Ther 2003; 306: 821–7.

Treuting PM, Snyder JM, Ikeno Y, Schofield PN, Ward JM, Sundberg JP. The vital role of pathology in improving reproducibility and translational relevance of aging studies in rodents. Vet Pathol 2016; 53: 244–9.

van Praag H, Schinder AF, Christie BR, Toni N, Palmer TD, Gage FH. Functional neurogenesis in the adult hippocampus. Nature 2002; 415: 1030–4.

Ward JM, Schofield PN, Sundberg JP. Reproducibility of histopathological findings in experimental pathology of the mouse: a sorry tail. Lab Animal 2017; 46: 146–51.

Weingarten M, Lockwood A, Hwo S, Kirschner M. A protein factor essential for microtubule assembly. Proc Nat Acad Sci USA 1975; 72: 1858–62.

Wilhelmsson U, Faiz M, de Pablo Y, Sjöqvist M, Andersson D, Widestrand A, et al. Astrocytes negatively regulate neurogenesis through the Jagged1-mediated Notch pathway. Stem Cells 2012; 30: 2320–9.

Wischik CM, Novak M, Edwards PC, Klug A, Tichelaar W, Crowther RA. Structural characterization of the core of the paired helical filament of Alzheimer disease. Proc Natl Acad Sci USA 1988; 85: 4884–8.

Wischik CM, Edwards PC, Lai RY, Gertz HN, Xuereb JH, Paykel ES, et al. Quantitative analysis of tau protein in paired helical filament preparations: implications for the role of tau protein phosphorylation in PHF assembly in Alzheimer's disease. Neurobiol Aging 1995; 16: 418–31.

Wischik CM, Edwards PC, Lai RY, Roth M, Harrington CR. Selective inhibition of Alzheimer disease-like tau aggregation by phenothiazines. Proc Natl Acad Sci USA 1996; 93: 11213–8.

Whitehouse PJ, Price DL, Struble RG, Clark AW, Coyle JT, Delon MR. Alzheimer's disease and senile dementia: loss of neurons in the basal forebrain. Science 1982; 215: 1237–9.

Wilkinson DG, Passmore AP, Bullock R, Hopker SWE, Smith R, Potocnik FC, et al. A multinational, randomised, 12-week, comparative study of donepezil and rivastigmine in patients with mild to moderate Alzheimer's disease. Int J Clin Pract 2002; 56: 441–6.

Yanamandra K, Jiang H, Mahan T, Maloney S, Wozniak D, Diamond M, et al. Anti-tau antibody reduces insoluble tau and decreases brain atrophy. Ann Clin Transl Neurol 2015; 2: 278–88.

Yoshiyama Y, Higuchi M, Zhang B, Huang S, Iwata N, Saido T, et al. Synapse loss and microglial activation precede tangles in a P301S tauopathy mouse model. Neuron 2007; 53: 337–51.

Zhang Y, Chen K, Sloan SA, Bennett ML, Scholze AR, O'Keeffe S, et al. An RNA-sequencing transcriptome and splicing database of glia, neurons, and vascular cells of the cerebral cortex. J Neurosci 2014; 34: 11929–47.